Blood Oxygen Level-dependent MRI for Evaluation of Early Response of Liver Tumors to Chemoembolization: an Animal Study

JIN WOO CHOI[1*], HYEONJIN KIM[2*], HYO-CHEOL KIM[1], YUNJUNG LEE[2], JEONGMIN KWON[2], ROH-EUL YOO[1], HYE RIM CHO[1], SEUNG HONG CHOI[1] and JIN WOOK CHUNG[1]

[1]*Department of Radiology, Seoul National University Hospital, Seoul National University College of Medicine, Seoul, Republic of Korea;*
[2]*Department of Medical Sciences, Seoul National University College of Medicine, Seoul, Republic of Korea*

Abstract. *Aim: To evaluate the feasibility of carbogen-challenge blood oxygen level-dependent (BOLD) magnetic resonance imaging (MRI) for assessing the early response of liver tumors to chemoembolization in a rat hepatoma model. Materials and Methods: In a 9.4-Tesla scanner, a multiple gradient-recalled echo sequence was utilized for R2* measurement at 11 and 13 days after tumor implantation, first during room air breathing and then with carbogen gas (95% O2/5% CO_2) breathing, to calculate the percentage changes of R2* values [ΔR2*(%)]. Transarterial chemoembolization was conducted 12 days after tumor implantation. Results: The ΔR2* value of the tumors was 10.61±8.94% on pre-chemoembolization images and −0.16±1.85% on post-chemoembolization images. There was a significant difference in the ΔR2* value of the tumors between pre-chemoembolization and post-chemoembolization BOLD MRI (p=0.013). Conclusion: Carbogen-challenge BOLD MRI can be a non-invasive and useful method for the evaluation of early response of liver tumors to chemoembolization.*

Transarterial chemoembolization is one of the mainstay treatments for hepatocellular carcinomas (HCC) that are ineligible for both surgery and percutaneous ablation (1, 2). In particular, chemoembolization is one of the only non-curative treatments that improve patient survival, along with sorafenib (2). In addition, chemoembolization has recently been improved by the use of drug-eluting beads as embolic and drug delivery agents instead of conventional iodized oil. Furthermore, various combination strategies in addition to chemoembolization have been widely studied. In particular, combinations with radiofrequency ablation or sorafenib are showing promising results in the latest literature (3-5). Paradoxically, despite these various remedies for HCC, finding the best option among them for each patient and each tumor type is becoming a new concern for clinicians. In other words, the accurate assessment of tumor stage, adequate decision of treatment method, early evaluation of treatment response, and timely modification of treatment strategy are warranted in the era of tailored treatment of HCC. Therefore, many radiologists have actively investigated tools for the precise and early assessment of treatment response.

Blood oxygen level-dependent (BOLD) magnetic resonance imaging (MRI) has been utilized as a sensitive and non-invasive tool to monitor the oxygenation state and blood perfusion of tissue, especially in functional MRI of the brain (6-8). Recently, BOLD MRI has also shown promise for the non-invasive demonstration of tumor oxygenation state (9-11). This state-of- the art technique has been in the limelight as a potentially useful method to assess tissue oxygenation state, address tissue perfusion, and predict treatment response of a tumor (12, 13). Rodrigues *et al*. reported that carbogen-challenge BOLD MRI can be a prognostic indicator of acute radiotherapeutic response in rodent tumors (14), which indicates the usefulness of BOLD MRI in tumor oxygenation state assessment. In terms of the liver, Guo *et al*. demonstrated that the carbogen-challenge BOLD MRI signal was well-correlated to tumor microvessel density in a rat hepatoma model (15), which suggests the potential of BOLD MRI to provide a surrogate marker of tumor microperfusion.

Accordingly, we believe that the BOLD MRI technique can be a robust tool for assessing liver tumor treatment response after chemoembolization because chemoembolization

*These Authors share first authorship.

Correspondence to: Hyo-Cheol Kim, MD, Department of Radiology, Seoul National University Hospital, # 28 Yongon-dong, Chongno-gu, Seoul, 110-744, Korea. Tel: +82 220722584, Fax: +82 27436385, e-mail: angiointervention@gmail.com

Key Words: Hepatocellular carcinoma, chemoembolization, blood oxygen level-dependent MRI.

substantially compromises tumor perfusion and induces subsequent hypoxia in treated tumors. Carbogen-challenge BOLD MRI can demonstrate differences between treated lesions, where oxyhemoglobin cannot arrive at the target due to arterial embolization, and naïve lesions, where oxyhemoglobin can reach the target and act as an endogenous contrast agent. However, to our knowledge, no study has evaluated carbogen-challenge BOLD MRI in assessing early response of liver tumors to chemoembolization.

The purpose of our study was to evaluate the feasibility of carbogen-challenge BOLD MRI for assessing the early response of liver tumors to chemoembolization in a rat hepatoma model.

Materials and Methods

Tumor cell line. The McA-RH7777 rat hepatoma cell line (CRL-1601; ATCC; Manassas, VA, USA) was obtained and cultured in Dulbecco's modified Eagle's medium (DMEM, WelGENE, Daegu, Korea), supplemented with 10% fetal bovine serum (WelGENE) and 1% penicillin-streptomycin mixture (Gibco, Grand Island, NY, USA). McA-RH7777 cells were cultured loosely adherent in culture flasks at 37˚C in a humidified atmosphere containing 5% CO_2. Trypan blue staining was conducted before each tumor implantation procedure to verify >90% cell viability.

Animal model. This study was approved by our Institutional Animal Care and Use Committee (#0720120670) and performed in accordance with institutional guidelines. Thirteen Sprague-Dawley (SD) rats (weight range, 300-350 g; Koatech, Pyeongtaek, Gyunggi-do, Korea) were used for our study. The subjects were anesthetized by injecting a solution of zolazepam (5 mg/kg, Zoletil®; Virbac, Carros, France) and xylazine (10 mg/kg, Rompun®; Bayer-Schering Pharma, Berlin, Germany) into the hindlimb. After anesthesia, a right-sided transverse mini-laparotomy was performed, and 1×10^7 McA-RH7777 rat hepatoma cells prepared in 50 μl of serum-free DMEM were gently injected under the hepatic capsule into the right medial lobe (16). Handheld cautery (Bovie Medical Corporation, Clearwater, FL, USA) was applied to prevent bleeding and cell reflux. The abdominal incisions were then closed with a two-layer technique.

Transarterial chemoembolization. Rats with hepatoma ≥9 mm on pre-chemoembolization MRI (11 days after tumor implantation) underwent transarterial chemoembolization by an experienced interventional radiologist (H. Kim.) at 12 days after tumor implantation. After anesthesia was achieved by the same method used for tumor implantation, a 2-cm longitudinal left paramedial incision was made in the neck. The left common carotid artery was exposed and cannulated by a 22-gauge intravenous catheter. After that, a custom-modified 1.5 Fr microcatheter (Marathon; EV3, Irvine, CA, USA) and a 0.010-inch guidewire (Silverspeed-10; EV3, Irvine, CA, USA) was inserted through the cannula, and the proper hepatic artery was selected under the guidance of fluoroscopy (16). A mixture of iodinated contrast agent and drug-eluting beads (100-300 μm, DC bead®; Biocompatibles, Surrey, UK) loaded with doxorubicin was infused until stasis was achieved on fluoroscopy. The microcatheter was then removed, and the carotid artery was ligated. The neck incision was sutured with a one-layer technique.

MRI acquisition. All MRI acquisitions were performed by two of the authors (H. Kim. and Y. L.) using a 9.4-Tesla MR scanner (Agilent 9.4T/160AS horizontal imaging system; Agilent Technologies, Santa Clara, CA, USA) with a volume coil for both radiofrequency transmission and signal reception (Agilent Technologies) at 11 days (pre-chemoembolization imaging) and 13 days (post-chemoembolization imaging) after tumor implantation. Before MRI, the rats were placed in a small chamber and anesthetized with 1.5% isoflurane in pure O_2 gas. Anesthesia was maintained with either 1.5% isoflurane in room air (78% N_2/20% O_2) or 1.5% isoflurane in carbogen gas (95% O_2/5% CO_2) during MRI scanning. Real-time monitoring of the animals' respiration and rectal temperatures was conducted during image acquisition. Initially, scout images were acquired in all three directions using a gradient echo sequence with the following imaging parameters: repetition time (TR)/echo time (TE)=79/2.7 ms; flip angle (FA)=30˚; 1 average; slice thickness (TH)=2 mm; no interslice gap; field-of-view (FOV)=65×65 mm^2; matrix size=128×128; receiver bandwidth=50 kHz. After automated, local shimming over the liver, fat-saturated axial T2-weighted spin-echo images (TR/TE=1000/30 ms; FA=90˚; 1 average; TH=2-mm; no interslice gap; typical FOV=62×35 mm^2; matrix size=128×128; receiver bandwidth=50 kHz) under free breathing of 1.5% isoflurane and room air (78% N2/20% O_2) were obtained for tumor localization. If a hepatoma ≥9 mm in diameter was confirmed on the T2-weighted MRI, four slices covering the tumor were defined for gas-challenge BOLD MRI with a respiratory-gated multiple gradient-recalled echo sequence with fat saturation (TR=5000 ms; TE=1.6, 5, 10, 15, 20, 25, 30, 35, 40 ms; FA=90˚; 2 averages; TH=2-mm; typical interslice gap=0.5-mm; typical FOV=58×35 mm^2; matrix size=128×128; receiver bandwidth=100 kHz). BOLD MRI was first obtained during 1.5% isoflurane and room air (78% N2/20% O_2) breathing; next, 1.5% isoflurane and carbogen gas (95% O_2/5% CO_2) was administered for a 10-minute interscan interval; finally, a second batch of BOLD MRI was acquired during 1.5% isoflurane and carbogen gas breathing. All breathing gases were administered *via* a rat nose cone at a rate of 1 liter per minute.

Image analysis. Image post-processing and analysis were performed by two authors (J.W.C. and J.K.) using Matlab software (Math Works, Inc., Natrick, MA, USA). Among the four image slices per each imaging session (pre-chemoembolization, post-chemoembolization), the best image slice minimally affected by motion artifacts and susceptibility artifacts from the adjacent organs (bowel, lung) and extracorporeal air was selected for postprocessing in consensus of the two authors. Voxel-wise R2* (1/T2*) maps during each gas inhalation (*i.e.* room air, carbogen) and each imaging session (*i.e.* pre-chemoembolization, post-chemoembolization) were calculated assuming monoexponential decay [*i.e.* $S(TEi) = S(0)\bullet\exp(-R2^*\times TEi)$]. On the R2* maps, a region-of-interest (ROI) for a hepatoma and an ROI for the liver parenchyma excluding the blood vessels were manually drawn to measure the mean R2* values. For each ROI (*i.e.* hepatoma, liver parenchyma), percentage changes in R2* [ΔR2*(%)] were calculated as follows:

$$\Delta R2^*(\%) = \frac{R2^*_{air} - R2^*_{carb}}{R2^*_{air}} \times 100$$

where $R2^*_{air}$ and $R2^*_{carb}$ are the R2* under room air challenge BOLD and under carbogen-challenge BOLD, respectively. Therefore, a total of four ΔR2* (%) values were calculated per

animal: liver of pre-chemoembolization, hepatoma of pre-chemoembolization, liver of post-chemoembolization, and hepatoma of post-chemoembolization.

Histological analysis. All rats were euthanized in a CO_2 chamber just after the post-chemoembolization BOLD imaging. Axial sections sampled across the center of the tumors were fixed in 10% buffered formaldehyde solution and paraffin embedded. After that, hematoxylin and eosin (H&E) staining was performed on each sample.

Statistical analysis. All statistical analyses were performed by one author (J.W.C.) using commercial software (IBM SPSS Statistics, version 19.0; SPSS Inc., IBM Company, Armonk, NY, USA). The differences in ΔR2* (%) values before and after chemoembolization were analyzed with a Wilcoxon signed rank test. A *p*-value of less than 0.05 was determined to indicate statistical significance.

Results

Eleven of the 13 rats implanted with McA-RH7777 cells had a hepatoma on pre-chemoembolization MRI (tumor induction rate, 84.6%). Therefore, chemoembolization *via* the left common carotid artery was performed in 11 rats, and the subjects also underwent pre- and post-chemoembolization BOLD MRI. There was no technical failure or mortality of chemoembolization. Before image post-processing, one subject was excluded from the analysis because substantial image deterioration by susceptibility artifacts was detected on pre-chemoembolization imaging. The 10 tumors finally analyzed in our study ranged from 9 to 12 mm [mean±standard deviation (SD), 10.8±1.2 mm] on pre-chemoembolization MRI. Tumors were identified as well-defined hyperintense lesions on T2-weighted images of both pre-chemoembolization and post-chemoembolization MRI. Gross specimens of the tumors revealed concordant solid masses, and subsequent H&E staining confirmed near total necrosis in all tumors.

According to room air and carbogen-challenge BOLD MRI, the mean ΔR2* value of the livers was 19.44% (SD=6.74%; range=12.40-31.31%) on pre-chemoembolization MRI and 15.60% (SD=6.96%; range=8.82-31.01%) on post-chemoembolization MRI. All ΔR2* values of the livers were positive on both pre-chemoembolization and post-chemoembolization BOLD MRI. Conversely, the mean ΔR2* value of the tumors was 10.61% (SD=8.94%; range=−8.61-21.64%) on pre-chemoembolization MRI and −0.16% (SD=1.85%; range=−3.91-2.13%) on post-chemoembolization MRI. One tumor showed a negative ΔR2* value (−8.61) on pre-chemoembolization BOLD MRI, and four tumors presented negative ΔR2* values on post-chemoembolization imaging. Detailed data for each rat are shown in Table I. From the results of the Wilcoxon signed rank test, there was a significant difference in the ΔR2* value of the tumor between pre-chemoembolization and post-chemoembolization BOLD MRI (p=0.013). However, the difference in the ΔR2* value of the liver was not significant (p=0.169). Representative BOLD MRI and corresponding ΔR2* maps are shown in Figure 1.

Table I. *The ΔR2* values for 10 rats that underwent pre-chemoembolization and post-chemoembolization blood oxygen level-dependent (BOLD) MRI.*

Subject no.	ΔR2* value (%)			
	Liver		Tumor	
	Pre-CE	Post-CE	Pre-CE	Post-CE
1	29.74	15.82	8.38	–3.91
2	22.76	12.89	17.64	0.21
3	16.33	13.97	9.87	0.21
4	31.31	10.92	16.60	–0.5
5	16.62	13.21	19.09	1.82
6	12.40	10.21	3.89	2.13
7	14.58	8.82	–8.61	–1.44
8	14.83	31.01	21.64	–1.77
9	13.79	14.32	6.14	0.07
10	22.01	24.80	11.43	1.57

CE, Chemoembolization; Note – The ΔR2* value is the percentage change of R2* values between room air and carbogen challenge BOLD MRI.

Discussion

In our study, chemoembolization induced a significant decrease in the ΔR2* value of the tumors on the day following the procedure (p=0.013). This finding is compatible with our hypothesis that arterial embolization blocks the arrival of oxyhemoglobin, which acts as an endogenous contrast agent in the tumor. Concordantly, all tumors in our study showed near total necrosis on H&E staining. In contrast, the ΔR2* values for the livers did not significantly decrease after chemoembolization (p=0.169), but there was a tendency for decline (19.44% to 15.60%). This finding may be the result of hepatic arterial occlusion by scattered DC beads because the selective chemoembolization of tumor-feeding arteries is technically impossible in the rat hepatoma model.

Meanwhile, if tumor-feeding arteries were embolized enough to induce total necrosis of the tumors, the ΔR2* value would have to be zero (*i.e.* no delivery of oxyhemoglobin) or a small positive number (*i.e.* minimal delivery of oxyhemoglobin). Therefore, we interpreted the small negative ΔR2* values for the tumors (−3.91, −0.50, −1.44, −1.77) on post-chemoembolization BOLD MRI as the result of image noise and minor artifacts. However, one tumor showed a substantial negative ΔR2* value (−8.61) on pre-chemoembolization imaging. This result may be due to the steal phenomenon of oxyhemoglobin from the tumor to the liver (17), which can be explained by the relatively effective

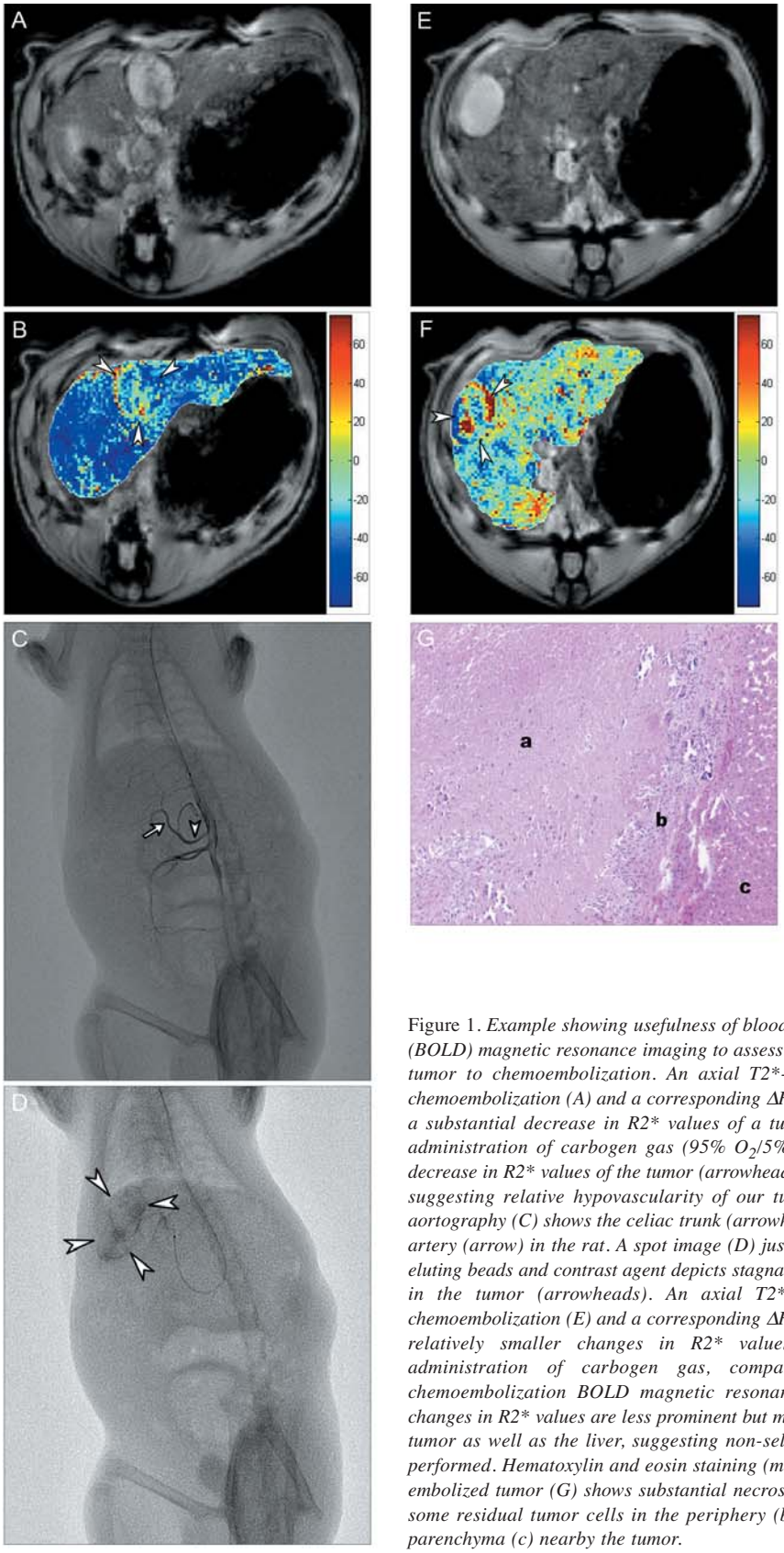

Figure 1. *Example showing usefulness of blood oxygen level-dependent (BOLD) magnetic resonance imaging to assess early response of a liver tumor to chemoembolization. An axial T2*-weighted image before chemoembolization (A) and a corresponding ΔR2* map (B) demonstrate a substantial decrease in R2* values of a tumor (arrowheads) after administration of carbogen gas (95% O_2/5% CO_2). Note the lesser decrease in R2* values of the tumor (arrowheads) compared to the liver, suggesting relative hypovascularity of our tumor model. Abdominal aortography (C) shows the celiac trunk (arrowhead) and proper hepatic artery (arrow) in the rat. A spot image (D) just after injection of drug-eluting beads and contrast agent depicts stagnation of the contrast agent in the tumor (arrowheads). An axial T2*-weighted image after chemoembolization (E) and a corresponding ΔR2* map (F) demonstrate relatively smaller changes in R2* values of the tumor after administration of carbogen gas, compared to that of pre-chemoembolization BOLD magnetic resonance imaging. Note that changes in R2* values are less prominent but more heterogeneous in the tumor as well as the liver, suggesting non-selective embolization was performed. Hematoxylin and eosin staining (magnification, ×10) of the embolized tumor (G) shows substantial necrosis of the tumor (a), with some residual tumor cells in the periphery (b), and the normal liver parenchyma (c) nearby the tumor.*

vasodilatation in normal liver vasculature during carbogen gas administration, compared with that of tumor neovasculature. In addition, although we conducted experiments with the same imaging protocol for all rats, the ΔR2* values of the tumors on pre-chemoembolization BOLD MRI were variable (range=−8.61-21.64%). We believe that these variations may reflect different tumor microenvironments such as tumor vascularity, blood supply ratio of the hepatic artery to the portal vein, and aerobic metabolic activity (15, 18, 19).

The modified Response Evaluation Criteria in Solid Tumors (mRECIST) and the European Association for the Study of the Liver (EASL) with contrast-enhanced computed tomography (CT) or MRI have played a pivotal role in the evaluation of HCC treatment response (20-22). However, changes in tumor size assessed by the above-mentioned criteria are not as effective as we can predict efficacy of the treatment at the early stage of the therapy when the tumor size is not changed (23). Furthermore, these approaches rarely provide information about tumor microenvironments, such as cellularity and hypoxic states. Although diffusion-weighted imaging (DWI) is referred to as a promising alternative to conventional response evaluation systems, some studies have demonstrated that DWI is less sensitive than contrast-enhanced MRI in assessing chemoembolization response (24, 25). However, contrast-enhanced MRI also has limitations. As it requires the administration of contrast agents, imaging must be carefully applied in patients with impaired renal function and does not allow for serial repetitive measurements in a short period of time.

In contrast, BOLD MRI is a simple and non-invasive tool, which does not require conventional contrast agent administration in order to assess chemoembolization response of HCC. In addition, because occlusion of the tumor-feeding arteries and subsequent hypoxic changes may occur immediately after the procedure, BOLD MRI can allow for adequate evaluation of early response of chemoembolization. Furthermore, carbogen gas is generally believed to be safe for humans and is even used during radiation therapy to increase the radiosensitivity of anoxic regions (26). Therefore, we believe carbogen-challenge BOLD MRI to be a very promising and safe tool for the evaluation of early response after chemoembolization.

However, the interpretation of BOLD MRI may be difficult in some situations. For example, a decrease in the ΔR2* value between room air and carbogen-challenge BOLD MRI may result from decreased tissue perfusion, improved tissue oxygenation in a baseline state, extremely increased oxygen consumption in a tissue, or mixtures of these above-mentioned states. Therefore, combining the technique with other MRI sequences can be useful for interpreting BOLD MR signals. In particular, arterial spin labeling (ASL) and intravoxel incoherent motion (IVIM) techniques, which can also assess tissue perfusion without the use of a contrast agent, may complement the use of BOLD MRI.

On the other hand, optimal BOLD pulse sequences in human MR scanners should be investigated in consideration of the image quality and acquisition time. Although current 1.5-Tesla or 3.0-Tesla clinical MR scanners can be less sensitive to changes in T2* than high-field animal MR scanners, human MR study has its advantages because breath-hold examinations can be performed, which greatly reduce the potential for motion artifacts and signal loss in abdominal images. The liver is an especially suitable candidate for BOLD imaging due to the following reasons: the liver is a very hypervascular organ, containing a substantial amount of oxyhemoglobin and deoxyhemoglobin, which serve as endogenous contrast agents, and in the normal liver, portal venous blood, which is more deoxygenated than arterial blood, is a major source of hepatic perfusion, providing a substantial response range to changes in tissue oxygenation (27). Indeed, promising results have been reported in human liver studies, as well as in animal research (28, 29). We hope that further human studies will optimize BOLD MRI protocols and evaluate the usefulness of BOLD imaging for early response evaluation after chemoembolization.

Our study has certain limitations. Firstly, we studied a small number of rats. However, our results demonstrated a statistically significant difference, which can also be explained by the theory behind chemoembolization. Therefore, we believe our sample size was sufficient to draw conclusions with minimal animal sacrifice. Secondly, we did not perform a perfusion study. BOLD MRI in conjunction with perfusion imaging, such as contrast enhanced MR, ASL, or IVIM techniques, may have provided a better understanding of tumor oxygenation status, as well as tumor perfusion, and thus a more in-depth assessment of tumor biology.

In conclusion, carbogen-challenge BOLD MRI can be a non-invasive and useful method for the evaluation of early response of liver tumors to chemoembolization.

Acknowledgements

This study was supported by a grant from the National R&D Program for Cancer Control, Ministry of Health & Welfare, Republic of Korea (1220040).

References

1 Bruix J, Sherman M and American Association for the Study of Liver Disease: Management of hepatocellular carcinoma: An update. Hepatology *53(3)*: 1020-1022, 2011.

2 Forner A, Llovet JM and Bruix J: Hepatocellular carcinoma. Lancet *379(9822)*: 1245-1255, 2012.

3 Kang SG, Yoon CJ, Jeong SH, Kim JW, Lee SH, Lee KH and Kim YH: Single-session combined therapy with chemoembolization and radiofrequency ablation in hepatocellular carcinoma less than or equal to 5 cm: a preliminary study. J Vasc Interv Radiol *20(12)*: 1570-1577, 2009.

4 Pawlik TM, Reyes DK, Cosgrove D, Kamel IR, Bhagat N and Geschwind JF: Phase II trial of sorafenib combined with concurrent transarterial chemoembolization with drug-eluting beads for hepatocellular carcinoma. J Clin Oncol *29(30)*: 3960-3967, 2011.

5 Cheng BQ, Jia CQ, Liu CT, Fan W, Wang QL, Zhang ZL and Yi CG: Chemoembolization combined with radiofrequency ablation for patients with hepatocellular carcinoma larger than 3 cm: A randomized controlled trial. JAMA *299(14)*: 1669-1677, 2008.

6 Ogawa S, Lee TM, Kay AR and Tank DW: Brain magnetic resonance imaging with contrast dependent on blood oxygenation. Proc Natl Acd Sci USA *87(24)*: 9868-9872, 1990.

7 Kwong KK, Belliveau JW, Chesler DA, Goldberg IE, Weisskoff RM, Poncelet BP, Kennedy DN, Hoppel BE, Cohen MS and Turner R: Dynamic magnetic resonance imaging of human brain activity during primary sensory stimulation. Proc Natl Acd Sci USA *89(12)*: 5675-5679, 1992.

8 Davis TL, Kwong KK, Weisskoff RM and Rosen BR: Calibrated functional MRI: Mapping the dynamics of oxidative metabolism. Proc Natl Acd Sci USA *95(4)*: 1834-1839, 1998.

9 Dunn JF, O'Hara JA, Zaim-Wadghiri Y, Lei H, Meyerand ME, Grinberg OY, Hou H, Hoopes PJ, Demidenko E and Swartz HM: Changes in oxygenation of intracranial tumors with carbogen: A BOLD MRI and EPR oximetry study. J Magn Reson Imaging *16(5)*: 511-521, 2002.

10 Hoskin PJ, Carnell DM, Taylor NJ, Smith RE, Stirling JJ, Daley FM, Saunders MI, Bentzen SM, Collins DJ, d'Arcy JA and Padhani AP: Hypoxia in prostate cancer: Correlation of BOLD-MRI with pimonidazole immunohistochemistry-initial observations. Int J Radiat Oncol Biol Phys *68(4)*: 1065-1071, 2007.

11 Taylor NJ, Baddeley H, Goodchild KA, Powel ME, Thoumine M, Culver LA, Stirling JJ, Saunders MI, Hoskin PJ, Philips H, Padhani AR and Griffiths JR: BOLD MRI of human tumor oxygenation during carbogen breathing. J Magn Reson Imaging *14(2)*: 156-163, 2001.

12 Gallez B, Baudelet C and Jordan BF: Assessment of tumor oxygenation by electron paramagnetic resonance: Principles and applications. NMR Biomed *17(5)*: 240-262, 2004.

13 Figueiras RG, Padhani AR, Goh VJ, Vilanova JC, Gonzalez SB, Martin CV, Caamano AG, Naveira AB and Choyke PJ: Novel oncologic drugs: What they do and how they affect images. Radiographics *31(7)*: 2059-2091, 2011.

14 Rodrigues LM, Howe FA, Griffiths JR and Robinson SP: Tumor R2* is a prognostic indicator of acute radiotherapeutic response in rodent tumors. J Magn Reson Imaging *19(4)*: 482-488, 2004.

15 Guo Y, Jin N, Klein R, Nicolai J, Yang GY, Omary RA and Larson AC: Gas challenge-blood oxygen level-dependent (GC-BOLD) MRI in the rat Novikoff hepatoma model. Magn Reson Imaging *30(1)*: 133-138, 2012.

16 Cho HR, Choi JW, Kim HC, Song YS, Kim GM, Son KR and Chung JW: Sprague-Dawley rats bearing McA-RH7777 cells for study of hepatoma and transarterial chemoembolization. Anticancer Res 33(1): 223-230, 2013.

17 Hsu YY, Chang CN, Jung SM, Lim KE, Huang JC, Fang SY and Liu HL: Blood oxygenation level-dependent MRI of cerebral gliomas during breath holding. J Magn Reson Imaging *19(2)*: 160-167, 2004.

18 Thomas CD, Chenu E, Walczak C, Plessis MJ, Perin F and Volk A: Relationship between tumour growth rate and carbogen-based functional MRI for a chemically induced HCC in mice. MAGMA *17*: 271-280, 2004.

19 Dunn TJ, Braun RD, Rhemus WE, Rosner GL, Secomb TW, Tozer GM, Chaplin DJ and Dewhirst MW: The effects of hyperoxic and hypercarbic gases on tumour blood flow. Br J Cancer *80*: 117-126, 1999.

20 Bruix J, Sherman M, Llovet JM, Beaugrand M, Lencioni R, Burroughs AK, Christensen E, Pagliaro L, Colombo M, Rodes J and EASL Panel of Experts on HCC: Clinical management of hepatocellular carcinoma. Conclusions of the Barcelona-2000 EASL conference. European Association for the Study of the Liver. J Hepatol *35(3)*: 421-430, 2001.

21 Lencioni R and Llovet JM: Modified RECIST (mRECIST) assessment for hepatocellular carcinoma. Semin Liver Dis *30(1)*: 52-60, 2010.

22 Shim JH, Lee HC, Kim SO, Shin YM, Kim KM, Lim YS and Suh DJ: Which response criteria best help predict survival of patients with hepatocellular carcinoma following chemoembolization? A validation study of old and new models. Radiology *262(2)*: 708-718, 2012.

23 Georgiades C, Geschwind JF, Harrison N, Hines-Peralta A, Liapi E, Hong K, Wu Z, Kamel I and Frangakis C: Lack of response after initial chemoembolization for hepatocellular carcinoma: Does it predict failure of subsequent treatment? Radiology *265*: 115-123, 2012.

24 Mannelli L, Kim S, Hajdu CH, Babb JS, Clark TW and Taouli B: Assessment of tumor necrosis of hepatocellular carcinoma after chemoembolization: Diffusion-weighted and contrast-enhanced MRI with histopathologic correlation of the explanted liver. AJR Am J Roentgenol *193(4)*: 1044-1052, 2009.

25 Kamel IR, Liapi E, Reyes DK, Zahurak M, Bluemke DA and Geschwind JF: Unresectable hepatocellular carcinoma: Serial early vascular and cellular changes after transarterial chemoembolization as detected with MR imaging. Radiology *250(2)*: 466-473, 2009.

26 Powell ME, Collingridge DR, Saunders MI, Hoskin PJ, Hill SA and Chaplin DJ: Improvement in human tumour oxygenation with carbogen of varying carbon dioxide concentrations. Radiother Oncol *50(2)*: 167-171, 1999.

27 Barash H, Gross E, Matot I, Edrei Y, Tsarfaty G, Spira G, Vlodavsky I, Galun E and Abramovitch R: Functional MR imaging during hypercapnia and hyperoxia: Noninvasive tool for monitoring changes in liver perfusion and hemodynamics in a rat model. Radiology *243(3)*: 727-735, 2007.

28 Fan Z, Elzibak A, Boylan C and Noseworthy MD: Blood oxygen level-dependent magnetic resonance imaging of the human liver: Preliminary results. J Comput Assist Tomogr *34(4)*: 523-531, 2010.

29 Haque M, Koktzoglou I, Li W, Carbray J and Prasad P: Functional MRI of liver using BOLD MRI: Effect of glucose. J Magn Reson Imaging *32(4)*: 988-991, 2010.

Received March 3, 2013
Revised April 8, 2013
Accepted April 9, 2013